HHS Public Access

Author manuscript

Min Metall Explor. Author manuscript; available in PMC 2024 May 24.

Published in final edited form as:

Min Metall Explor. 2021 May 13; 38(4): 1739–1759. doi:10.1007/s42461-021-00430-x.

Assessing Longwall Gateroad Ground Response and Support Alternatives

Gabriel S. Esterhuizen[1], **Ted Klemetti**[1], **Morgan M. Sears**[1], **Peter Zhang**[1], **Mark van Dyke**[1], **Heather Dougherty**[1], **I. Berk Tulu**[2]

[1]National Institute for Occupational Safety and Health, Pittsburgh, PA, USA

[2]West Virginia University, Morgantown, WV, USA

Abstract

Ground falls in longwall gateroad entries remain a concern in modern longwall operations. The gateroads are subject to changing horizontal and vertical ground stress induced by longwall extraction. These stress changes can result in failure of the strata around an entry leading to large deformations of the entry roof, floor, and ribs. The gateroad support systems are required to control the failed strata while maintaining safe access to the longwall face and unimpeded ventilation. This paper presents research that was conducted to better understand the stability issues in gateroad excavations and to develop procedures for evaluating support and layout alternatives for longwall gateroads. Using the results of a field-monitoring program and numerical model analysis of case histories, a conceptual model of gateroad support needs was developed. The conceptual model formed the basis for developing a set of equations that can be used to estimate likely roof sag and support loading for given roof geology and longwall-induced loading conditions. The developed equations were used to compare predicted gateroad stability to field study results, showing satisfactory agreement. The calculation procedures are used to demonstrate their application in assessing support alternatives at a case study mine. It is concluded that the developed analysis procedures provide realistic assessments of likely ground stability and can be used to evaluate alternative gateroad support systems at operating longwall mines.

Keywords

Longwall; Ground control; Gateroad; Support design; Monitoring; Numerical modeling

1 Introduction

Ground falls in underground coal mines in the USA accounted for 12.9% of reported lost-time injuries and 29.7% of fatalities during the 5-year period of 2015 to 2019 [1].

Gabriel S. Esterhuizen, eee5@cdc.gov.

Conflict of Interest The authors declare no competing interests.

Disclaimer The findings and conclusions in this report are those of the authors and do not necessarily represent the official position of the National Institute for Occupational Safety and Health, Centers for Disease Control and Prevention. Mention of any company or product does not constitute endorsement by NIOSH.

Achieving adequate ground control in longwall gateroad entries is especially challenging because these excavations are subject to changing loads induced by longwall extraction that can result in large deformation of the roof, ribs, and floor strata [2, 3]. In addition, the geologic composition of the roof can vary considerably along the length of a gateroad, resulting in variable ground response and support requirements [4, 5].

1.1 Gateroad Support Design Considerations

Designing appropriate support for the variable geologic conditions and loading conditions typically encountered in a longwall gateroad is challenging because of the large number of parameters that affect the stability of the excavation. A further complication is the variable duration of longwall-induced loading. In some cases, the supports only need to control the roof for a relatively short period of time. For example, a longwall headgate belt entry may only be subject to the peak loading conditions for less than one day as the longwall face approaches and mines up to the supports. On the other hand, the support system in entries located between the gobs of two longwall panels may be required to control the ground for periods exceeding 2 years, while subject to extreme vertical stress conditions. Support required in a headgate gateroad with short-duration loading is very different from entry support requirements for longer term loading.

At present, gateroad support systems are largely designed based on historical experience in similar geologic and operational settings. Standing support selection can be facilitated by using the NIOSH-developed Support Technology Optimization Program (STOP) [6], which allows various commercially available standing support systems to be compared. The procedures described in this paper represent a further step in the development of gateroad support design procedures that allow designers to simultaneously consider many of the important parameters that affect gateroad stability.

1.2 Research Conducted

The research in this study was conducted through a combined program of data collection on current gateroad support practices, full-scale testing of gateroad support systems at the NIOSH Mine Roof Simulator; monitoring of longwall-induced ground deformation, stress changes, and support response at longwall operations in the USA; analysis of the results; and development of numerical modeling procedures that allow expected support performance and ground response to be evaluated. The developed numerical models were used to conduct parametric studies in which the important factors affecting entry stability under changing stress were evaluated. The understanding of gateroad stability derived from the results formed the basis of a conceptual model of support requirements in longwall gateroads. Using the conceptual model as a basis, the relationships between important input parameters for gateroad stability were derived through regression analysis of the results of the parametric studies. The derived relationships can be used by support designers to assess support alternatives for local geologic conditions and longwall-induced loads.

In this research, the need for surface control to prevent smaller rock fragments from falling between supports was not evaluated. The focus was on preventing large roof falls that would impede ventilation or safe access to the longwall working face. While the focus of this

research was on the impact of longwall-induced stress changes on entry stability, it must be noted that individual geologic structures such as slips or inclined joints and faults in the roof may result in local instability. These structures were not explicitly considered in the analyses nor in the proposed support assessment procedures.

This paper describes the key results of the field-monitoring program and the results of parametric studies that shaped the conceptual model of gateroad stability. The principles of the conceptual model are explained, and calculation procedures are proposed that allow the roof sag and expected support loading to be estimated for given geologic and longwall loading conditions. The results are compared to field-monitoring outcomes, and a case study mine is presented to demonstrate the application of the developed procedures.

2 Ground and Support Response Monitoring

The monitoring program was initiated in 2015 in which data were collected at operating longwall mines in Pennsylvania, West Virginia, Virginia, Wyoming, and Utah. The mines were operating in the Pittsburgh, Lower Kittanning, and Pocahontas seams, Sunnyside and in the D41 seam in Wyoming.

Monitoring sites were located either in the future tailgate entry or in the track entry. Monitoring initiated soon after development of gateroad entries and continued until longwall mining had passed on both sides of the gateroad. Initial deformation immediately behind the face of the entry during development was not captured by the instruments, but all changes caused by first and second panel mining were attempted to be measured. A summary of the longwall layout and support systems installed at six of the NIOSH monitoring sites is provided in Table 1. The immediate roof geology at the monitoring sites is illustrated in Fig. 1 demonstrating the variety of geological conditions included in the study. Data collected during previous NIOSH research at a Colorado mine in the D-seam [7] (mine D) and a Pennsylvania mine in the Pittsburgh coal bed [8] (mine E) were included in the study. Monitoring results from mines A, B, C, D, and E were used for model calibration. Mine F was used as a validation study. An additional published case study (Mine J) was included for validation where headgate deformations were measured by Lu and Hasenfus [9].

2.1 Mine Site Instrumentation

The desired set of instruments for each gateroad monitoring site is shown schematically in Fig. 2. It was not possible to install the full set of instruments at all monitoring sites because of practical limitations related to access and timing in high production longwall environments. The instrumentation had the objective to measure stress changes, strata deformations, and support loading induced by longwall extraction. Instrument installation was conducted during development at the time of installation of the supports and was wired-up to dataloggers as soon as through ventilation was achieved.

Three-dimensional stress changes in the roof strata were measured using the CSIRO Hollow Inclusion Cell (HI-cell) [10] typically at locations indicated in Fig. 2. Vertical stress changes in the unmined coal adjacent to the gateroad entry were measured using borehole pressure cells (BPCs) that were originally developed through US Bureau of Mines research and were

manufactured locally according to NIOSH specification. The BPCs are fitted with pressure transducers that have an accuracy of 0.25% of range. In this research, BPC results were only used to assess trends in loading, rather than attempting to derive absolute stress-change values.

Roof deformation was measured using multiple point borehole extensometers (MPBX) that were manufactured by NIOSH technicians at the Pittsburgh Mining Research Laboratory. The relative displacement between the anchor and the borehole collar is measured using a linear transducer with 10 cm of travel and resolution of 0.25 mm. Up to eight monitoring wires were installed in the boreholes, with anchor points at selected locations depending on geology and length of roof bolts. Measuring points were located up to 6 m above the entry roof.

Deformation of the coal ribs was measured using multiple point borehole extensometers of various designs. Currently extensometers manufactured by Mine Design Technologies and RST Instruments Ltd. are used that have up to six monitoring points. Deformations are measured using linear potentiometers with up to 500 mm of stroke and ± 2% linearity. Rib deformation anchor points were located between 1.8 and 9.0 m horizontally into the coal bed being mined.

The loading of the cable bolt supports was measured by using cable-bolt load cells (GEOKON Model 3000) installed with 25 mm thick bearing plates at the collar of the cable bolt supports. The load cells use electrical resistance strain gauges with 0.025% full-scale accuracy under laboratory conditions. Four to eight cable bolts were instrumented at each monitoring site.

Standing support loads were measured using a modified Hydrocell (Strata Worldwide) standing support prestressing unit. The unit is a water-filled welded bladder made of expandable sheet-metal that is installed underneath or on top of the support and is equipped with a commercially available pressure transducer that has 1% accuracy. Standing support deformation was measured using various commercially available string potentiometers mounted within about 15 cm of the top and bottom of the standing supports as dictated by local conditions. The potentiometers have an accuracy of 0.25% of full scale.

Instrument calibrations are conducted prior to installation at mine sites. Most instruments such as the HI-cells and cable bolt load cells arrive with manufacturer provided calibration factors, temperature deviation corrections, zero offsets and other instrument specific factors. Calibrations for pressure transducers are conducted internally following ASTM Standard Specifications. The standing support load cells are calibrated using the NIOSH Mine Roof Simulator through the full range of anticipated in-mine loading. The displacement monitoring devices are calibrated to 0.025 mm using a precision caliper.

Dataloggers used for the studies were the Campbell Scientific 21X for the HI-cells and the MIDAS (Golder Associates) originally developed by NIOSH.

2.2 Roof Sag Monitoring Results

Figure 3 summarizes key roof sag monitoring results measured in track and tailgate entries at five of the NIOSH monitored instrumentation sites. It was observed that after development and before the impact of the approaching longwall face becomes evident, the roof is essentially stationary. As the first longwall panel approaches and passes by the monitoring instruments, roof deformations are typically less than 35 mm. The roof sag increases up to about 100 mm at the tailgate corner as the second longwall mines up to the instruments. These deformations are small relative to the yield capacity of standing supports but may approach or exceed the yield limit of cable bolts.

Much larger roof sag measurements have been reported in poor ground or unfavorable stress conditions caused by the orientation of gateroads relative to the major horizontal stress. Lu and Hasenfus [9] measured average roof sag of 150 mm at the headgate corner of a longwall panel that was unfavorably oriented to the major horizontal ground stress. Under these conditions, extreme support measures were required that included installing supplementary 6-m-long cable bolts and injecting polyurethane to stabilize the roof.

In most of the monitored cases, during the periods when the longwall face was remote from the monitoring sites, no roof sag was detected. However, in two cases, mine C and to a lesser extent at mine A in Fig. 3, creep-like roof sag was measured, which appeared to be associated with the presence of clay-rich sediments such as claystone in the roof. These creep-like movements ranged from approximately 1 mm to 10 mm per month.

Since the roof is more than adequately supported during development, gravity-driven bending or sagging of the roof is arrested by the support system. Except for time-dependent, creep-like deformations, the roof deformation observed as the longwall face approaches can be assumed to be driven by stress-induced failure of the roof strata.

2.3 Bolt and Cable Loading Monitoring Results

Loading and deformation of the fully grouted bolts was not measured because of practical difficulties and regulatory requirements. Cable bolts are usually not fully grouted, and it was possible to measure cable bolt loading using load cells installed between the cable bolt faceplate and the rock face. Initial cable bolt loads during the development stage varied between about 10 kN and 50 kN. As the longwall-induced load increased, cable bolts that were 3.6 m long loaded-up rapidly and achieved their maximum loads after about 75 mm to 100 mm of roof sag. It was found that the cable bolts' stiffness calculated from field results were lower than those derived from controlled tests. In the field, the measured stiffness of the cable bolts was 2.24 kN/mm compared to 3.50 kN/mm typically measured in controlled tests [11]. The lower stiffness of the cable bolts provides further support for the observation that under small initial roof deformations the contribution of cable bolts will be less than the contribution of the much stiffer fully grouted bolts.

2.4 Standing Support Monitoring Results

Standing support load and deformation measurements confirmed loading of the standing supports and were used to derive floor heave from the roof-to-floor convergence

measurements. This also provided insight into the load transfer from cable bolts to standing supports as the roof deformation increases. Figure 4 shows how longwall-induced roof deformation causes cable bolts to achieve their peak load and start shedding load soon after the longwall face had mined past the monitoring location. As the cable bolts shed load, the weight of detached strata is transferred to the standing supports resulting in a rapid increase in loading of the standing supports. The cable bolts may appear to be redundant under these loading conditions, however, they provide support to the roof from the development stage to the time that standing supports are installed. They also provide interior reinforcement to resist unraveling of the fractured and failed roof strata.

3 Numerical Modeling Studies

Monitoring rock mass response and support performance in the field is costly and time consuming. In this research, numerical model analyses were used to supplement field data with information about support system performance under geologic and stress conditions beyond those that were measured in the field. The FLAC3D V5.1 finite difference software [12] was used to conduct the modeling studies. The models were initially calibrated against the in-mine monitoring results and the calibrated models were used to conduct parametric studies that investigated the impact of changes in loading, geology, and support systems on gateroad entry stability.

3.1 Numerical Modeling Procedures

Modeling procedures were developed to investigate both regional stability concerns associated with longwall mining, and local stability issues associated with coal mine entries [2, 13-15]. Models were created at three different scales: the longwall panel scale, the longwall district scale, and the entry scale. Initially the panel-scale models were used to investigate the interactions between the approaching longwall face and gateroad entries. The models were large and took several days to solve for the numerous mining increments needed to capture the longwall induced loading-path of the gateroads. In addition, the panel-scale models could not efficiently model details of the local roof geology and installed supports to conduct meaningful comparative analyses. Consequently, entry-scale models were created that had sufficient detail to model the local roof response and support system interactions. The effect of an approaching longwall on entry stability was simulated by imposing the longwall-induced loading path on the entry model. The loading path was determined either by in-mine monitoring or by the district-scale models.

Model calibration was achieved by developing standardized procedures for estimating the required inputs for the models. Procedures were developed for estimating field-scale rock properties from laboratory tests, for initiating the pre-mining ground stress within the various layers, and for simulating the caved gob behind the longwall face. Through an iterative process, the panel-scale models were calibrated against field monitoring results of abutment stress extent, pillar loading and surface subsidence [2]. For entry-scale models, further calibration was needed because of the change in scale of the models. Model results were calibrated against in-mine extensometer readings and bolt and standing support loading measured at the NIOSH monitoring sites [11, 14, 16]. The main calibration parameters were

the rock mass and gob properties that cannot be tested in the laboratory. Support systems are modeled using the strength and deformation parameters as tested in controlled laboratory or in-mine measurements [17]. Grout properties were calibrated against laboratory and in-mine monitoring as described by Tulu et al. [18]. The standardized procedures for creating model inputs were applied to all further numerical modeling studies.

3.2 Panel-Scale Model Layout and Analysis

Figure 5 illustrates a panel-scale model demonstrating the model extents and typical excavation details. The model represents two longwall panels with planes of symmetry located along the longitudinal center line of each panel. The model sides were free to move in the vertical direction, while the bottom of the model was fixed. The top of the model is a free surface representing the ground surface. Geologic layers were explicitly modeled as strain-softening ubiquitous joint materials to capture strength anisotropy related to bedding within strata units. Contacts between strata layers were modeled as joint interfaces that follow the Coulomb sliding model, allowing both sliding and separation to occur. Table 2 presents a selection of material types and interfaces ranging from weak to strong, and their mechanical properties as used in the models. The caved gob was modeled as a strain-hardening material extending vertically from the mined floor to three times the mining height and was introduced behind the longwall face as the face was advanced in the models, as described by Tulu et al. [2].

Initial model loading was based on gravity loading in the vertical direction and horizontal stress was initiated using local stress measurement results or according to Mark and Gadde [19] if local measurements were not available. The model was run by first establishing a state of equilibrium prior to mining. The gateroads were excavated next as a single excavation step and solved to equilibrium. The first longwall was then partially excavated as a single step followed by a series of ten mining increments of 5 m each to advance the face past the entries and crosscuts of interest. Gob was introduced in the void created behind the face as mining progressed. For each mining increment the internal unbalanced forces were gradually reduced to avoid shock loading of the system. The process was repeated for the second longwall to investigate gateroad response to tailgate loading conditions. The panel-scale modeling results were evaluated to develop an understanding of the interactions between the gateroad and the longwall, with particular attention being paid to the height of potential roof failure over intersections, crosscuts, and entries. Figure 6 is an example of the results illustrating a close-up view of roof sag in entries and crosscuts near the longwall face.

3.3 Longwall District and Entry-Scale Modeling

The district-scale models were created using the same procedures and inputs as described for the panel-scale models except that the district-scale models could simulate the sequential extraction of several longwall panels. Larger element sizes were used to achieve reasonable run times. The stress distributions and overburden deformations were verified against field measurements to ensure that the models were sufficiently accurate at calculating the stress redistribution in the areas of interest around the longwall panels. Figure 7 shows the layout of such a model indicating the model extents and grid meshing on the coal horizon. The longwall-induced stress path in the roof strata of the gateroad entries was determined

by extracting the changes in the vertical and horizontal stress components in the plane perpendicular to the entry direction. The calculated stress-path was applied to the detailed entry-scale models.

The entry-scale models simulated a vertical cross section through an entry that has a horizontal thickness equal to a multiple of the support spacing. Typically, the model thickness was 2.4 m. The models used the same constitutive models and modeling approach described earlier. However, in these models, geologic units as thin as 15 cm were modeled, allowing details of the complex geologic layering at many of the case-study sites to be captured adequately. During the calibration studies it was found necessary to account for the weakening effect caused by delamination of bedded rock units in the low confinement zone that exists in the immediate roof of an excavation. This was achieved by considering the "bedding rating" as a parameter to define field-scale strata strength under low confinement [14]. The bedding rating is determined from the Coal Mine Roof Rating (CMRR) [20] and is the sum of the bedding shear strength rating and bedding intensity ratings.

Bolts and cable bolts were modeled using the finite-element structural elements available in FLAC3D. Table 3 presents an example of the mechanical properties of a fully grouted bolt and calibrated resin grout properties used in these models. Standing supports were modeled as passive supports installed after the initial roof sag associated with entry development had occurred. Standing support loads were, therefore, generated by roof deformation induced by the approaching longwall face. The standing supports are simulated by a Coulomb strain-softening/hardening material that follows the load-deformation curve of the full-scale standing supports as tested in the NIOSH mine roof simulator [17].

An example of an entry-scale model layout is shown in Fig. 8. The bottom of the model is fixed, and the sides are free to slide in the vertical direction. Load is applied to the top of the model equal to the overburden load. A plane-strain condition was assumed by inhibiting displacements out of the plane of the section. The modeling sequence is as follows: initialize pre-mining vertical and horizontal stress, run the model to initial equilibrium in the pre-mining state, extract the entry, gradually reduce the unbalanced forces to zero to maintain a quasi-static condition. Bolting is installed when the unbalanced forces have reduced by 70%. The objective is for the bolts to experience deformation that would be associated with development of the entry. Standing supports are installed in the model after the development equilibrium state is achieved. Figure 8 also shows a close-up view of an entry model with bolts, cable bolts, and standing supports installed. After the development stage has been solved, the entry is subject to the desired longwall-induced stress path by applying vertical and horizontal loads to the model in a quasi-static manner. The model is loaded in the vertical direction by applying the longwall-induced loads in small increments along the top of the model while the desired horizontal stress changes are applied by velocity boundaries along the sides of the model.

Figure 9 shows an example of typical entry model results indicating rock mass damage, the resulting rock mass deformation, and support loading. The rock mass damage shown in Fig. 9a illustrates how several rock failure modes are captured by the models and how a dome of failing rock is formed above the entry. Figure 9b shows the same entry at a later stage

of loading, where the cable bolts have failed, and the failing roof rock is now resting on the standing supports. The load in the bolts and cable bolts is shown, as well as the stress within the standing supports. The models also captured the formation of roof cutters and subsequent cantilevering of the roof. Figure 9b shows the formation of cutters at the right and left corners of the roof.

This approach for modeling longwall-induced strata deformations and entry stability was used during the model calibration studies and produced realistic ground deformations, extent of strata failure, and support loads when compared to in-mine monitoring results [11, 16]. The standardized modeling approach was used to conduct further investigations and parametric studies of gateroad stability.

4 Parametric Studies of Factors Affecting Gateroad Stability

The parametric studies considered various geologic scenarios, depths of cover, longwall induced stress paths, and support systems. More than 2000 combinations of parameters and loading conditions were simulated.

4.1 Geologic Scenarios Evaluated

The parametric studies considered ten different geologic scenarios. Five of the scenarios were based on actual mine sites where field monitoring was conducted, and five generic scenarios were created to investigate specific geological settings. Table 4 lists the ten geological scenarios and the depth of cover ranges considered.

4.2 Depth of Cover and Horizontal Stress Scenarios

The numerical models were set to simulate depths of cover ranging from 180 m to 600 m. Not all geologic scenarios were assessed at all depths of cover because the weaker roof cases collapsed under development conditions at the greater depths. The models were subject to a series of stress increments of 2 MPa each to simulate the loading path induced by an approaching longwall panel. The stress increments were selected to provide horizontal-to-vertical stress increment ratios of between 0.33 and 3.0. For each analysis, the stress was increased until the roof sag in the model exceeded 300 mm or the stress increase exceeded 30 MPa, which represents the likely range of loading conditions in the longwall panels monitored.

4.3 Support Systems Evaluated

Support systems consisted of roof rock reinforcement by fully grouted bolts or fully grouted bolts and cable bolts. Supplemental support using various types of standing supports was also modeled. The roof reinforcement consisted of various combinations of 1.8-m and 2.4-m-long fully grouted bolts with peak tensile strength of 180 kN. Cable bolts with lengths of 3.0 m, 3.6 m, and 4.9 m and maximum tensile strength of 270 kN were modeled.

Standing supports were modeled as passive supports installed after the initial roof sag associated with entry development had occurred. Standing support loads were, therefore, generated by roof deformation induced by the approaching longwall face. The load-

deformation curve for the standing supports was based on testing results obtained at the NIOSH Mine Roof Simulator and presented in the STOP software. Support types evaluated included: 9-point timber cribs, engineered timber cribs, engineered timber props, and cementitious yieldable cribs of various capacities. The supports modeled represent the typical range of standing support capacities currently used in US longwall gateroads.

5 Key Results of Parametric Studies

The results of the parametric studies provided useful insight into some of the aspects of roof-support interaction that are difficult to determine from field studies. For example, a support and loading system can easily be tested in exactly the same geology and loading conditions using numerical models, while this is almost impossible to achieve in real-world field studies. Two sets of insightful results are presented below.

5.1 Impact of Horizontal Stress

The model results indicated that the change in horizontal stress caused by longwall mining has a significant impact on roof stability in the gateroads. This may explain why the majority of longwall panels in the eastern USA are oriented to ensure that the horizontal stress impact is minimized. Figure 10 shows numerical-model-predicted roof sag results for a gateroad at a depth of 240 m in the Pittsburgh coal bed subject to variable longwall-induced horizontal-to-vertical stress ratios. The horizontal stress component perpendicular to the entry direction is considered in these models. The charts show results up to the loading stage just prior to roof collapse. The results demonstrate how higher horizontal stress increments can produce significantly greater roof deformation and consequently increased roof instability. These results help to explain why managing horizontal stress is one of the major considerations when laying out new longwall districts [21].

5.2 Impact of Support Systems

Quantifying the impact of different types of supports on roof sag and roof stability was a major objective of the parametric studies. Figure 11 shows modeling results for a gateroad in the Pittsburgh coal bed at 240-m depth of cover that is subject to increasing longwall-induced stress. Six different support scenarios were modeled, and the resulting roof sag is shown against the longwall-induced vertical stress. Results for the standing supports are shown up to the loading stage where roof sag exceeds 25 cm, while the bolt and cable bolt results are again shown only up to the loading stage just prior to roof collapse.

The support systems consisted first of four 1.8-m fully grouted bolts in rows 1.2 m apart. Then, two 3.6-m-long cable bolts were added and evaluated. The cable bolts had 1.2 m of grout at the upper end with a free length of 2.4 m. The further analyses all had the same bolt and cable bolt configuration supplemented by different standing support types. The results demonstrate the reduction in roof sag achieved by the various support systems. The improvements when adding cable bolts to fully grouted bolts is clearly demonstrated. Adding standing supports further limits roof sag. Early installation of standing supports will, therefore, improve roof conditions by limiting deformation and dilation of the roof. The analyses showed that the difference in roof sag between various types of standing

supports is less obvious. Field observations have also shown a minor difference in roof sag with different types of standing supports [22]. However, most standing support systems are able to control the damaged roof that would otherwise have collapsed. This can only be achieved if the standing supports are able to yield to the longwall-induced deformations while maintaining adequate support load.

6 Conceptual Model of Ground-Support Interaction

The results of the field-monitoring studies and the numerical model analyses were reviewed to develop a conceptual model of the interaction between the roof strata and the gateroad support system [23]. The conceptual model presents an interpretation of ground and support interaction in response to longwall-induced loading. Using this model together with information about expected longwall-induced loading and roof sag, the effect of alternative support systems on roof stability can be assessed by simple calculations [17].

6.1 Basic Premises of the Conceptual Model

The conceptual model was developed on the premise that the support system is required to control the detached roof strata that would collapse in the absence of any support. The conceptual model subdivides the roof strata into three categories: intact strata that are undamaged by mining-induced effects, failing strata that have been loaded beyond their peak strength but have sufficient residual strength to be self-supporting, and (c) detached strata that would collapse in the absence of support. The dead weight of the detached strata, therefore, represents the load that must be controlled by the support system.

Mining-induced roof sag is used as the main indicator of roof stability. For the conceptual model, any roof sag that occurs after initial development is assumed to be caused by the approaching longwall. The longwall-induced loads result in failure of the roof strata, which in turn results in dilation of the rock. The roof dilation forces the roof downwards and is observed as roof sag. The support system will influence the roof sag and height of detached roof depending on time of installation and support capacity. The effect of coal rib failure and floor heave on roof sag are indirectly included in the model results but were not explicitly evaluated. Creeprelated deformations were not considered in this study.

6.2 Sequence of Ground-Support Interaction Events

The response of a gateroad entry and support system to the effect of longwall-induced loading is illustrated in Fig. 12. The loading stages and support response may be described as follows:

- **a.** The initial condition is a stable entry under development loading conditions that is reinforced by bolts and/or cable bolts. At this stage, the roof sag is likely to have generated tension in the bolts and cable bolts. The fully grouted bolts are carrying a greater load because they are stiffer than the cable bolts.
- **b.** The approaching longwall face induces horizontal and vertical stress changes in the surrounding rock, which causes an increase in the degree and height of failed roof strata and causes the lower roof to become detached. Dilation of the new

fractures within the failing roof drives the roof downwards. Cutter formation on one side of the entry may result in the formation of a detached cantilever in the roof. The detached roof is suspended by the bolts and cable bolts.

c. Continued loading causes the detached roof to extend beyond the bolts which causes them to start losing their reinforcement and suspension ability. Suspension is now provided mainly by the cable bolts. Standing supports may have been installed, and they carry some of the detached roof load depending on the convergence experienced by the standing supports.

d. As the longwall-induced load continues to increase, the bolts become fully encapsulated in the detached roof and have limited reinforcing effect. The cable bolts may yield if they are extended beyond their elastic limit or the dead weight of the detached roof exceeds their ultimate tensile strength. The standing supports now carry the major load of the detached roof. Floor heave may occur which further compresses the standing supports and may also increase their loading.

According to this model, the success of a support system can be assessed if the height of detached roof and the amount of roof deformation are known. The height of detached roof determines the dead weight that must be supported. The deformation determines the survival of the bolts and cable bolts against elongation failure and determines the response generated in standing supports.

7 Calculation Procedures

Following the principles of the conceptual model, it is necessary to determine the likely longwall-induced stress changes and calculate the resulting roof deformation and the height of detached roof. The success of a support system can then be assessed based on its ability to control the detached roof and accommodate the expected roof deformation.

The field-monitoring results and the results of the parametric studies were used to derive a series of equations to estimate the roof sag and height of detached roof using the expected longwall-induced stress changes as input. The longwall-induced stress changes can be estimated from the results of field measurements under similar geologic conditions or by conducting numerical model analyses. For example, Tulu et al. [2] present procedures for modeling longwall panels, the overburden strata, and the longwall gob suitable for estimating longwall-induced gateroad loading.

7.1 Estimating Roof Sag

An equation to estimate the longwall-induced roof sag at the entry roof line was derived by multiple linear regression analysis of the parametric study results. The effects of the independent variables were initially assessed to establish which parameters have the most significant impact on roof sag. Parameters that were strongly correlated were combined to reduce interactions in the analysis, while parameters with limited impact on the roof sag were eliminated. Any variables that had p-values above 0.05 (indicating limited significance) were eliminated.

The final seven parameters selected for roof sag estimation were as follows, in descending order of importance: (1) longwall-induced horizontal stress, (2) initial horizontal stress in the entry roof, (3) field-scale strength of the roof strata within the fully grouted bolt horizon, (4) field-scale strength of the roof strata in the cable-bolt anchorage horizon, (5) longwall-induced vertical stress, (6) standing support capacity, and (7) reinforcement capacity (bolts and cable bolts). The regression equation to predict roof sag has a coefficient of determination (r^2) value of 0.78 with a root mean square error of 12 mm.

The regression analysis showed, not unexpectedly, that the parameters that have the greatest impact on roof sag are the stress state and the roof strength, while the support system has a lesser effect. The limited impact of the support system on the longwall-induced roof sag can be explained by the fact that the equivalent pressure exerted by the support system distributed over the full width of the entry is about two orders of magnitude less than the longwall-induced stress that drives the roof strata failure and associated dilation. In-mine monitoring has also shown that changes in standing support systems appear to have limited impact on roof deformations induced by longwall mining [22]. However, the success of the standing supports depends on their ability to maintain sufficient load bearing capacity in spite of the convergence imposed on them by the deforming strata.

The resulting equation to estimate the roof sag (s) in centimeters at the roof line of a gateroad entry has three components:

$$s = (\mathrm{S1} + \mathrm{S2} + \mathrm{S3} + C)^2 \tag{1}$$

where S1 represents the stress state, S2 represents the roof strength, S3 represents the support efficiency, and C is a constant determined from the regression analysis. Each component is calculated as follows:

$$\mathrm{S1} = 0.1345 \times \mathrm{Hinc} + 0.0319 \times \mathrm{Vinc} + 0.279 \times \mathrm{SIGHini} \tag{2}$$

$$\mathrm{S2} = -0.117 \times \left(\frac{\mathrm{RSa}+2 \times \mathrm{RSi}}{3.0}\right) - 0.0126 \times \mathrm{RSc} \tag{3}$$

$$\mathrm{S3} = -0.0028 \times \mathrm{SSc} - 0.0023 \times (\mathrm{RRb} + \mathrm{RRc}) \tag{4}$$

$$C = 1.237 \tag{5}$$

where Hinc is the horizontal stress increase induced by the longwall panel (MPa), Vinc is the vertical stress increase (MPa) induced by the longwall panel, SIGHini is the initial horizontal stress in the roof strata (MPa) in the direction perpendicular to entry development, RSa is the weighted average field-scale strength of strata in the bolt anchorage zone (upper 60 cm of fully grouted bolts) (MPa), RSi is the weighted average field-scale strength of strata in the immediate roof (from roof line to start of bolt anchorage zone) (MPa), and RSc is the weighted average field-scale strength of strata in the cable anchorage zone (upper 1.2 m of cable bolts) (MPa). SSc is a parameter representing standing support efficiency, while RRb and RRc are parameters representing the roof reinforcement provided by bolts and cable bolts, respectively.

The field-scale strength of the different roof strata units is derived from the uniaxial compressive strength (UCS) of the rock matrix and the rating of bedding strength according to the CMRR, as described by Esterhuizen et al. [14, 24].

The effect of the fully grouted bolts (RRb) on roof sag is calculated after Mark et al. [25]:

$$\mathrm{RRb} = \frac{\mathrm{Nb} \times \mathrm{Lb} \times \mathrm{Cb}}{\mathrm{We} \times \mathrm{Sb}} \tag{6}$$

where Nb is the number of bolts per row, Lb is the bolt length (m), Cb is the bolt ultimate tensile capacity (kN), We is the width of the entry (m), and Sb is the spacing between rows of bolts (m).

The cable bolt effect (RRc) is also calculated using Eq. 6 but replacing bolt dimensions and capacities with the appropriate values for the cable bolts.

The standing support impact on roof sag is determined from the work capacity of the standing supports. This allows the peak and post-peak yield capacity of the different standing supports to be accounted for. The work capacity (SSw) is calculated as the average work (kN m) per cm of compression when compressing a standing support by 30 cm. Table 5 presents work capacity of some typical standing supports.

The standing support impact (SSc) is calculated as follows:

$$\mathrm{SSc} = \frac{\mathrm{SSw}}{\mathrm{Ns} \times \mathrm{Ss}} \tag{7}$$

where SSw is the average standing support work capacity over 30 cm of compression (kN m per cm), Ns is the number of standing supports in each row (typically one or two), and Ss is the center-to-center spacing between rows of standing supports (m).

7.2 Accounting for Entry Width and Intersection Effects on Roof Sag

Changes in the width of entries have a direct impact on roof deformation and stability. Intersections of two or more entries are generally less stable than single entries because larger roof spans are exposed, resulting in increased roof deformation and height of potential roof strata failure [26]. The results of initial modeling and analysis of intersections [27], combined with a review of field-measured data, were used to formulate a procedure to adjust for the effect of entry and intersection width on roof stability. The calculated roof sag (s) is modified to account for changes in the excavation width as follows:

$$s_w = 0.182 \times W \times s \tag{8}$$

where s_w is the width-adjusted roof sag, W is the entry width in meters (not the intersection dimension), and s is the roof sag in centimeters calculated by Eq. 1. The constant value of 0.182 in Eq. 8 will result in an adjustment factor of 1.0 when the entry width is 5.5 m, which was the base entry width used in the parametric studies.

The increased roof sag at intersections is estimated by setting W in Eq. 8 equal to 1.5 times the entry width for four-way intersections and 1.3 for three-way intersections. These increased excavation spans approximate the average diagonal spans at the intersections. These factors may be adjusted to assess the impact of increased intersection spans caused by coal sloughing at the pillar corners or poor mining practices.

7.3 Estimating the Height of Detached Roof

To obtain realistic estimates of the height of detached roof, statistics of actual roof falls were reviewed and compared to numerical model results in this study. Figure 13 shows the cumulative distribution of the height of reportable noninjury roof falls in US coal mines [28]. The maximum height of the reported roof falls is approximately equal to the typical 5 to 6-m width of entries found in US coal mines. The figure also shows the height of detached roof predicted by the numerical models conducted as part of this research. In the models, the height of detached roof was defined as the vertical distance from the centerline of the roof to a point where the sag exceeds 2.5 cm. The results show that there is a satisfactory agreement between the model outcomes and reported roof-fall heights.

Further evaluation of the model results showed that the height of detached roof was related to both the strength of the roof strata and the magnitude of roof sag measured at the entry roof line. The roof sag estimate adequately accounts for the effect of longwall-induced stress changes. The results also showed that the maximum height of roof strata failure is approximately the same as the entry width, similar to field observations. Observations and model results seem to indicate that the vertical growth of roof failure becomes limited as the failed zone achieves an arched shape.

An equation to estimate the height of detached roof (Y) in meters was derived from the results of the parametric study models. The equation is based on least squares error fitting an exponential curve to the modeling results for roof sag exceeding 2.5 cm:

$$Y = 1.34 \times SFR \times \ln(s_w) - 4.75 \times \ln(SFR \times 1.34) \quad (9)$$

where s_w is the width-adjusted roof sag (cm) using Eq. 8 and SFR is the thickness-weighted average safety factor of the roof strata units within 5 m of the entry roof. The safety factor of each strata unit is calculated as the ratio of the field scale strength of the strata unit to the horizontal component of the stress acting in the direction perpendicular to the long axis of the entry.

7.4 Assessing Bolt and Cable Bolt Performance

The roof sag and height of detached roof can be used to determine the expected loading and deformation of bolts and cable bolts. The approach presented here expresses support performance as a safety factor against failure of the supports. According to the conceptual model, failure by elongation, loss of anchorage, or overloading by the dead weight of the detached roof should be considered. The method of calculation and simplifying assumptions to facilitate these calculations are described below.

Failure by either loss of anchorage or overloading is both affected by the load sharing between bolts and cable bolts. A simplifying assumption was made that bolts and cable bolts share the dead weight of the detached roof in proportion to their axial stiffnesses.

Failure by elongation can occur if stress-driven fracturing and dilation of the roof elongates the bolt and cable bolt support units beyond their tensile strain limit. The safety factor against elongation failure is calculated as the ratio of the elongation limit of the support to the expected amount of roof sag. The study results showed that the typical 1.8-m-long fully grouted bolts are unlikely to fail by elongation because they become encapsulated by the detached roof before they reach critical elongation. Once encapsulated by the detached roof, they will sag within the roof strata without significant increase in elongation. The cable bolts, with their greater length, are more likely to fail by elongation.

Failure by loss of anchorage can occur if the detached roof encroaches on the anchorage zone of the supports and reduces the anchorage capacity. The anchorage zone is assumed to be the upper 60 cm of the solid bar bolts and 1.2 m for cable bolts. The load-carrying capacity of the bolts was assumed to linearly decrease from full capacity to zero as the height of detached roof reaches from 60 cm below to 60 cm above the top of the bolts. This assumption is partially justified by the study of reported roof falls [28], which showed that 69% of reported roof falls extend between 0 and 60 cm above the top of the bolted horizon. This seems to indicate that bolts become ineffective as the detached roof extends more than 60 cm above the bolted horizon. The safety factor against loss of anchorage is calculated as the ratio of anchorage capacity to the share of dead weight load carried by the supports.

If the supports do not fail by elongation or loss of anchorage, they may fail by overloading. The safety factor against overloading is calculated as the ratio of the ultimate tensile strength of the supports to their share of the dead weight load.

7.5 Assessing Standing Support Performance

In these calculations, it was assumed that standing supports are initially passive and only respond to roof-to-floor convergence that occurs after installation. The longwall-induced roof sag is used to calculate the contribution of the roof to the convergence. The floor heave component of convergence is difficult to estimate because standing supports may punch the floor and would not be subject to the same amount of compression as the observed roof-to-floor convergence. A practical solution may be to assume that floor heave is a fixed percentage of the roof sag, based on knowledge of the floor geology and in-mine observations.

Standing support loads are determined from the estimated convergence and the load-deformation curve of the support as tested at the NIOSH Mine Roof Simulator and presented in the Support Technology Optimization Program (STOP) [6]. The safety factor of the standing supports is calculated as the ratio of the current capacity of the supports to the dead weight load of the detached roof rocks minus the portion of the dead weight borne by the roof reinforcement system (bolts and cable bolts). For supports with continuously increasing load capacity, such as 9-point timber cribs, the capacity is based on 15 cm of convergence.

7.6 Calculating the Overall Stability of the Roof

In accordance with the conceptual model, the stability of the roof depends on the ability of the support system to prevent the collapse of the detached roof strata. Therefore, the roof stability is expressed as a safety factor, which is the ratio of the support capacity to the dead weight of the potential detached roof.

Gateroads are usually supported using different support units, each with its own capacity. The maximum safety factor of the support units is used to represent the overall stability of the roof. The safety factor can be converted to an equivalent “roof stability rating” or similar parameter for ease of communication as presented in Esterhuizen et al. [23].

8 Verification of Calculation Procedures

The calculation procedures are verified by comparing predicted entry and support response against the original field measurements. Results are presented showing comparisons of roof sag, support load, and overall entry stability.

8.1 Roof Sag Verification

The ability of the presented calculation procedures to estimate roof sag is compared against field measurements at three NIOSH monitoring sites and one published case history that represent a variety of roof strengths and depths of cover. For the calculation of roof sag, the longwall-induced horizontal and vertical stress changes were estimated from numerical model results following the procedures outlined in this paper. The calculated results and field-measured roof sag are presented in Fig. 14, showing the effect of first panel and second panel mining. The results demonstrate that the calculation procedures adequately predict the large displacements associated with unfavorable horizontal stress and weak roof geology at a depth of 240 m measured by Lu and Hasenfus [9] at Mine J. The same procedures are able

to predict relatively minor displacements in a gateroad entry at mine B at a depth of 600 m in strong roof strata. The correlation between the calculated and measured roof sag for initial development, first panel loading, and second panel loading is shown in Fig. 15.

8.2 Support Loading Verification

At mine A, the monitoring instruments survived inby the face, and it was possible to measure load shedding of the cable bolts and transfer of load to the standing supports as the roof sag approached 100 mm [11]. Figure 4 shows the in-mine monitoring results for this case. The geotechnical and support data were used to calculate the expected roof sag in the tailgate as the second panel mined up to the entry. The roof sag for points inby the face is not predicted by the calculation procedures. For the inby points, the field-measured roof sag was used to demonstrate how the equations predict the support response. Results are presented in Fig. 16, which compares well to the field-measured support response presented in Fig. 4.

8.3 Verification Case Study

The ability of the calculation procedures to provide realistic estimates of overall roof stability is demonstrated by assessing a headgate roof fall at Mine F in the Pittsburgh coal bed. The gateroad consisted of three entries that were each 4.9-m wide. The overall width of the gateroad was 65 m consisting of 30-m-wide and 35-m-wide pillars, with the larger pillar against the tailgate entry.

8.3.1 Geotechnical Information—The roof strata at this mine are typical of the Pittsburgh coal bed and consist of alternating coal riders and claystone beds in the immediate 90 to 180 cm of the roof, overlain by moderate-strength shale grading to sandstone or limestone beds. At the location of the headgate roof fall, the roof geology was in a transition zone where the roof strata changed from a sandstone-with-shale environment to a limestone environment with underlying claystone. Transition zones are known for their difficult ground conditions [29, 30] because of the presence of the weak claystone beds in the roof. Additionally, the thinly bedded shale and sandstone units are susceptible to changes in the horizontal stress [5]. Figure 17a illustrates the roof composition determined by borescope logging in the proximity of the headgate roof fall, illustrating the presence of claystone in the cable bolt anchorage zone. For comparison, Fig. 17b also shows the roof composition at the NIOSH monitoring site that was located in the track entry in the same gateroad that had more typical roof geology.

Local rock strength data from the roof collapse area were not available. Consequently, representative uniaxial compressive strength (UCS) values were estimated using the extensive set of rock testing data for the Pittsburgh roof strata available at NIOSH. The rock strength and bedding strength used in the analyses are presented in Table 6. Detailed roof-scoping observations of the sedimentary features [5] were used to assist in estimating the CMRR bedding ratings for the strata units in the roof.

8.3.2 Roof Support System—The standard support system in the 4.9-m-wide headgate entries consisted of two 2.7-m-long, point-anchor combination bolts installed on a T3-channel with a single 17-mm-diameter cable bolt in the center of the strap that is 3.6-m

long. The support rows are 1.2 m apart. During longwall retreat, an additional 2.7-m bolt is installed every 1.2 m to protect the headgate walkway. After the roof fall occurred in the headgate belt entry, specialist contractors were brought in to inject resin grout to consolidate the roof. Two 4.9-m-long, pumpable cable bolts were additionally installed in rows 1.2 m apart between the rows of standard bolt supports. The supplementary support was able to successfully control the roof so that the longwall could advance through the transition zone after the roof fall had been cleaned-up.

8.3.3 Pre-mining Stress and Longwall-Induced Stress—The initial ground stress was calculated using the Mark and Gadde [19] procedure for estimating pre-mining horizontal stress in the eastern USA. The modeling procedures for district-scale modeling described in this paper were followed to estimate the longwall-induced horizontal and vertical stress 90 cm above the roof line of the headgate entry at the headgate corner. The results indicated the horizontal stress in the direction perpendicular to the headgate entry to be 13.5 MPa and the vertical stress to be 15.4 MPa,

8.3.4 Calculation of Roof Stability—The loading conditions at the headgate corner were used to assess the overall roof stability. Equations (1 and 9 are used to calculate the roof sag and the height of detached roof for both the transition zone and the normal roof geology in the headgate entries and at the three-way intersections. The performance of the bolt and cable bolt supports, and the overall stability of the roof were then calculated using the procedures described in this paper. A final calculation was carried out to determine the impact of the 4.9-m supplementary cable bolts that were installed during the recovery of the belt entry in the transition zone. The calculated safety factors of the headgate belt entry under the maximum loading conditions at the headgate corner are presented in Fig. 18. Results are shown for both the normal and transition zone geology.

In normal geology with the standard roof support the factor of safety of the headgate entries and intersections were calculated to be 1.89 and 1.36, indicating that satisfactory roof stability conditions should exist, as experienced at the mine. However, the results for the transition zone indicate that headgate stability using the standard support system would be questionable with factor of safety values of 1.09 for the entries and 0.70 at the intersections. This would indicate a high likelihood of a roof fall in headgate intersections in the transition zone and unsatisfactory stability in the straight entries.

Closer inspection of the results indicates that in the transition zone the height of detached roof will reduce the effectiveness of the 2.7-m-long bolts, and the dead weight of the detached roof strata would load the cable bolts near their limit. In the intersections, the height of roof failure is estimated to extend to 3.3 m above the roof line, which would reduce the effectiveness of the cable bolt anchorage and would overload the cable bolts. The height of detached roof predicted by the equations is similar to the estimated 3-m height of the roof fall observed when visiting the mine a few days after the roof-fall event.

Finally, Fig. 18 also shows that the plan to install supplementary supports consisting of two 4.9-m cable bolts every 1.2 m as an emergency measure is predicted to restore the factor of safety to 1.77 in the intersections and 2.30 in the intersections. These cable bolts are

successful because they extend beyond the estimated zone of roof strata failure and provide additional capacity to help carry the dead weight of the detached roof. The experience at the mine showed that the supplementary cable bolts were indeed successful to control the roof and allow longwall operations to be re-established.

9 Conclusions

Through this study, procedures to assess the stability of the roof of gateroad entries and intersections have been developed for use in evaluating support and layout alternatives for longwall gateroads. The calculation procedures are based on field studies of gateroad support performance at longwall operations, verification of numerical models against field results, and parametric studies using the developed numerical models. A conceptual model that describes roof stability under changing stress is presented that forms the basis for the calculation procedures. Regression equations are presented that estimate likely roof sag and the height of detached roof, which are then used to determine the support response and its capacity to control the roof. A factor of safety is calculated by comparing the support load-bearing capacity to the dead weight of the potentially detached roof. The calculation procedures allow the impact of support systems and mine-layout alternatives on roof stability to be assessed during the planning stage of a longwall operation without resorting to advanced numerical model analysis. This would make the outcome of the research available to front-line engineers at operating mines who do not have access to advanced numerical modeling methods.

A case study demonstrates that the calculation procedures would have correctly predicted a headgate roof fall while advancing a longwall through a geologic transition zone, and the success of the standard support system in normal geologic conditions would also have been indicated correctly. Finally, the procedures would have indicated that the planned supplementary support installed by the mine would produce stable roof conditions at the longwall headgate corner in the unfavorable transitional zone geology, as experienced in practice.

It is concluded that the developed analysis procedures provide realistic assessments of likely ground stability in longwall gateroads and can be used to evaluate alternative support systems.

Acknowledgements

The research was conducted as part of the research program of the Pittsburgh Mining Research Division of NIOSH. The authors wish to thank the mine staff at collaborating longwall operations for providing access to their mines and assisting with monitoring activities and providing feedback on analysis of the outcomes. This research would not have been possible without the expertise of the NIOSH technicians and support staff who prepared instruments, conducted installations, and maintained the instruments in the harsh mining environment.

References

1. NIOSH (2020) NIOSH Mining Data and Statistics, Web page: https://www.cdc.gov/niosh/mining/statistics/default.html

2. Tulu IB, Esterhuizen GS, Gearhart D, Klemetti TM, Mohamed KM, Su DWH (2017). Analysis of global and local stress changes in a longwall gateroad. In: Proceedings of the 36th International Conference on Ground Control in Mining, pp. 100–110.

3. Wade LV, Conroy PJ (1980) Rock mechanics study of a longwall panel. Min Eng 32(12):1728–1735

4. Su DW, Thomas EP, Hasenfus GJ (1999) Roof geology mapping in underground coal mines. In Proceedings of the 18th International Conference on Ground Control in Mining. West Virginia University, pp. 40–49.

5. Van Dyke M, Klemetti T (2019) Geologic data collection and assessment techniques in coal mining for ground control. In Proceedings of the 38th International Conference on Ground Control in Mining, p. 72. Society for Mining, Metallurgy & Exploration.

6. Barczak TM (2000) Optimizing secondary roof support with the NIOSH Support Technology Optimization Program (STOP). In: Proceedings of the 19th International Conference on Ground Control in Mining. Morgantown, WV, pp 74–84

7. Larson MK, Whyatt JK (2012) Load transfer distance calibration of a coal panel scale model: a case study. In Proceedings of the 31st International Conference on Ground Control in Mining. Morgantown, WV: West Virginia University.

8. Oyler D, Mark C, Gale W, Chen J (2004) Performance of roof support under high stress in a US coal mine. 2004 SME Annual Meeting, Feb 23-25, Denver, Colorado, preprint 04-135. Littleton, CO: Society for Mining, Metallurgy, and Exploration, Inc, 2004 Feb; :1–9.

9. Lu J, Hasenfus G (2019) Challenges of mining the first righthanded longwall panel in a new reserve block in Pittsburgh Seam. Int J Min Sci Technol 29(1):145–149

10. Worotnicki G (1993) CSIRO triaxial stress measurement cell. In Rock Testing and Site Characterization, pp. 329–394. Pergamon.

11. Esterhuizen GS, Gearhart DF, Tulu IB (2018) Analysis of monitored ground support and rock mass response in a longwall tailgate entry. Int J Min Sci Technol 28(1):43–51 [PubMed: 29644113]

12. Itasca Consulting Group (2014) FLAC3D Fast Lagrangian analysis of continua in 3 dimensions. Itasca Consulting Group, Minneapolis, MN

13. Esterhuizen GS, Bajpayee TS, Murphy MM, Ellenberger JL (2013) Evaluation of the strength reduction method for US coal mine entry stability analysis. In Proceedings of the Seventh International Symposium on Ground Support in Mining and Underground Construction. Australian Centre for Geomechanics:373–385

14. Esterhuizen GS, Tulu IB, Bajpayee TS (2017) Application of a brittle failure model to assess roof stability in coal mine entries. In: Proceedings of the 51st US Rock Mechanics/Geomechanics Symposium, American Rock Mechanics Association, Paper No. 17–444.

15. Tulu IB, Esterhuizen GS, Klemetti T, Murphy MM, Sumner J, Sloan M (2016) A case study of multi-seam coal mine entry stability analysis with strength reduction method. Int J Min Sci Technol 26(2):193–198 [PubMed: 28239503]

16. Esterhuizen GS, Gearhart DF, Klemetti T, Dougherty H, van Dyke M (2019) Analysis of gateroad stability at two longwall mines based on field monitoring results and numerical model analysis. Int J Min Sci Technol 29(1):35–43

17. Esterhuizen GS, Tulu IB, Barczak TM, Gearhart DF, Dougherty H, Van Dyke M (2020) Assessing support alternatives for longwall gateroads subject to changing stress. In 39th International Conference on Ground Control in Mining, Pittsburgh, PA. Society for Mining Metallurgy and Exploration, 15.

18. Tulu IB, Esterhuizen GS, Heasley KA (2012) Calibration of FLAC3D to simulate the shear resistance of fully grouted rock bolts. In 46th US Rock Mechanics/Geomechanics Symposium. American Rock Mechanics Association.

19. Mark C, Gadde M (2008) Global trends in coal mine horizontal stress measurements. In: Proceedings of the 27th International Conference on Ground Control in Mining. Morgantown, WV, p. 319–31.

20. Molinda GM, Mark C (1994) Coal mine roof rating (CMRR): A practical rock mass classification for coal mines. Pittsburgh, PA: U.S. Department of the Interior, Bureau of Mines, IC 9387. 83.

21. Su DWH, Hasenfus GJ (1995) Regional horizontal stress and its effect on longwall mining in the Northern Appalachian coal field. Proceedings of the 14th International Conference on Ground Control in Mining, Morgantown, WV, pp. 39–45

22. Mirabile B, Westman E (2019) Secondary support instrumentation in longwall ventilation entries. In Proceedings of the 38th International Conference on Ground Control in Mining, Morgantown, WV, p. 350.

23. Esterhuizen GS, Tulu IB, Barczak TM, Dougherty H (2020) Ground response and support interaction in coal mine longwall gateroads subject to changing stress. In 54th US Rock Mechanics Geomechanics Symposium, American Rock Mechanics Association. Paper 20–1251, 7.

24. Esterhuizen GS, Bajpayee TS, Ellenberger JL, Murphy MM (2013) Practical estimation of rock properties for modeling bedded coal mine strata using the Coal Mine Roof Rating. In Proceedings of the 47th US Rock Mechanics/ Geomechanics Symposium. American Rock Mechanics Association, pp 1634–1647.

25. Mark C, Molinda GM, Dolinar DR (2000) Analysis of roof bolt systems. In Proceedings of the 20th International Conference on Ground Control in Mining, Morgantown, WV, pp. 218–225.

26. Molinda G, Mark C, Bauer E, Babich D, Pappas D (1998) Factors influencing intersection stability in US coal mines. In Proceedings of the 17th International Conference on Ground Control in Mining, Morgantown, WV, pp. 267–275.

27. Esterhuizen GS, Tulu IB, Klemetti T (2014) Analysis of factors influencing coal mine intersection stability. In Proceedings of the 48th US Rock Mechanics/Geomechanics Symposium. American Rock Mechanics Association.

28. Bajpayee TS, Pappas DM, Ellenberger JL (2014) Roof instability: what reportable noninjury roof falls in underground coal mines can tell us. Prof Saf 59(3):57 [PubMed: 26435556]

29. Lu J, Van Dyke M, Su DW, Hasenfus G (2016) Transitional geology and its effects on development and longwall mining in Pittsburgh Seam. Int J Min Sci Technol 26(1):31–37

30. Zhang P, Gearhart D, Van Dyke M, Su D, Esterhuizen E, Tulu B (2019) Ground response to high horizontal stresses during longwall retreat and its implications for longwall headgate support. Int J Min Sci Technol 29(1):27–33

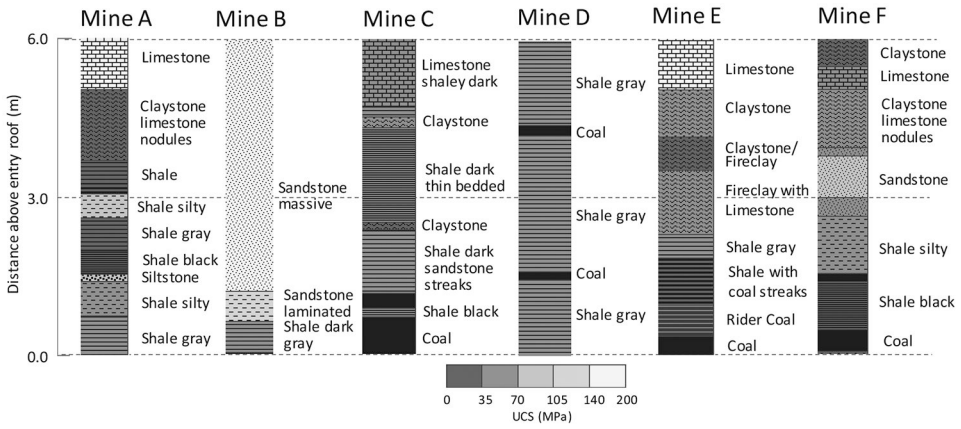

Fig. 1.

Summary of roof geology at six NIOSH gateroad monitoring sites. Shading indicates approximate range of intact rock strengths. Coal is shaded black

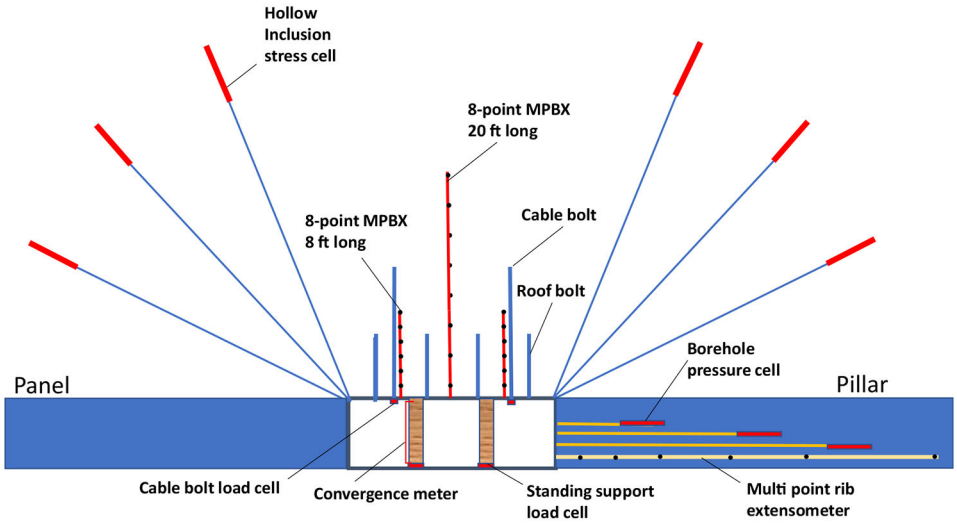

Fig. 2.
Illustration of desired instrument layout installed at gateroad monitoring sites

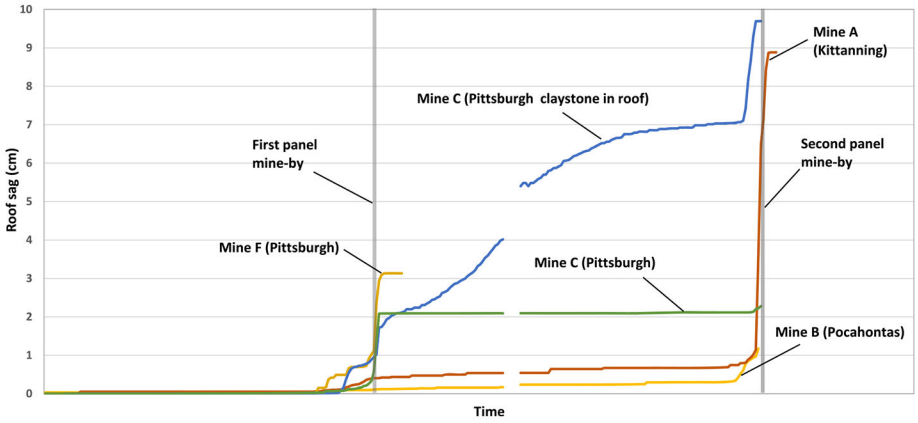

Fig. 3.
Roof sag measurements from five NIOSH monitoring sites showing a variety of results

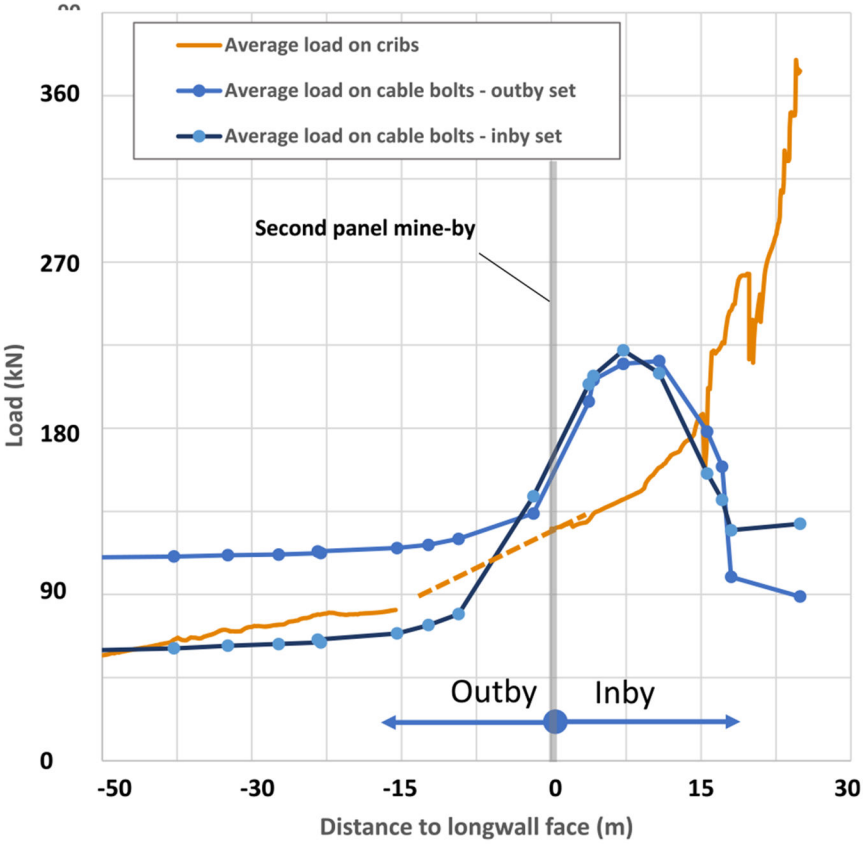

Fig. 4.

Average response of crib standing supports and two sets of cable bolts against the distance of the monitoring site to the advancing longwall face (Esterhuizen et al. [11])

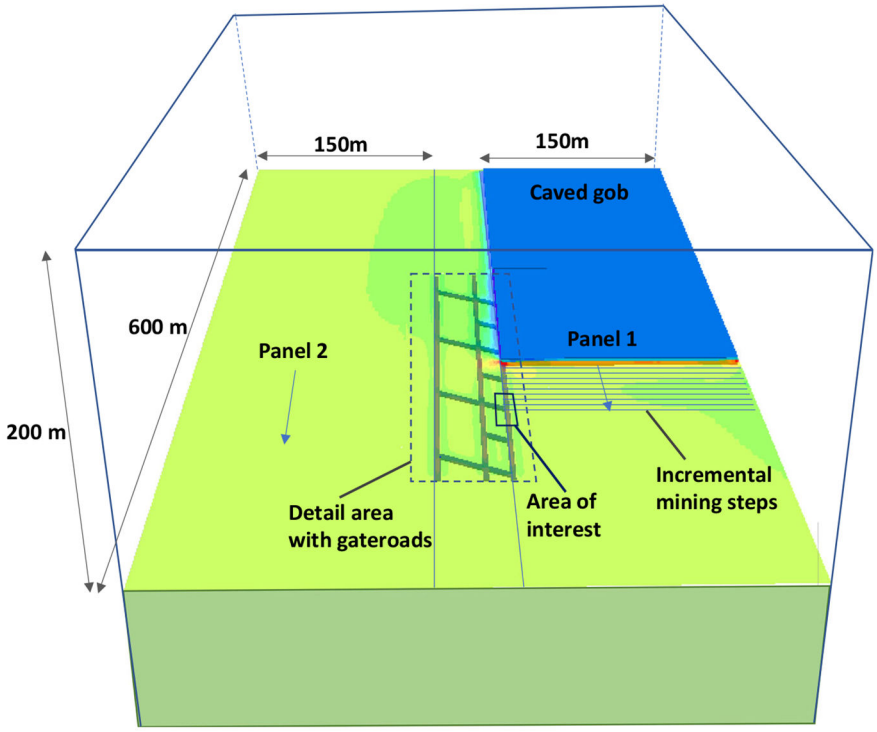

Fig. 5.

Layout of a panel-scale model showing first panel mining and headgate area of interest being evaluated

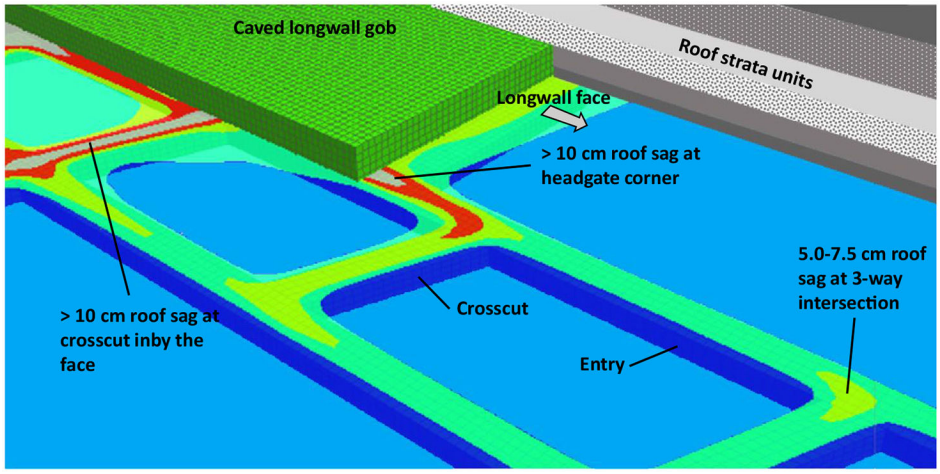

Fig. 6.

Cutaway view of a panel-scale model showing roof deformation contours 0.5 m above the roof of the gateroad development as the longwall approaches an intersection

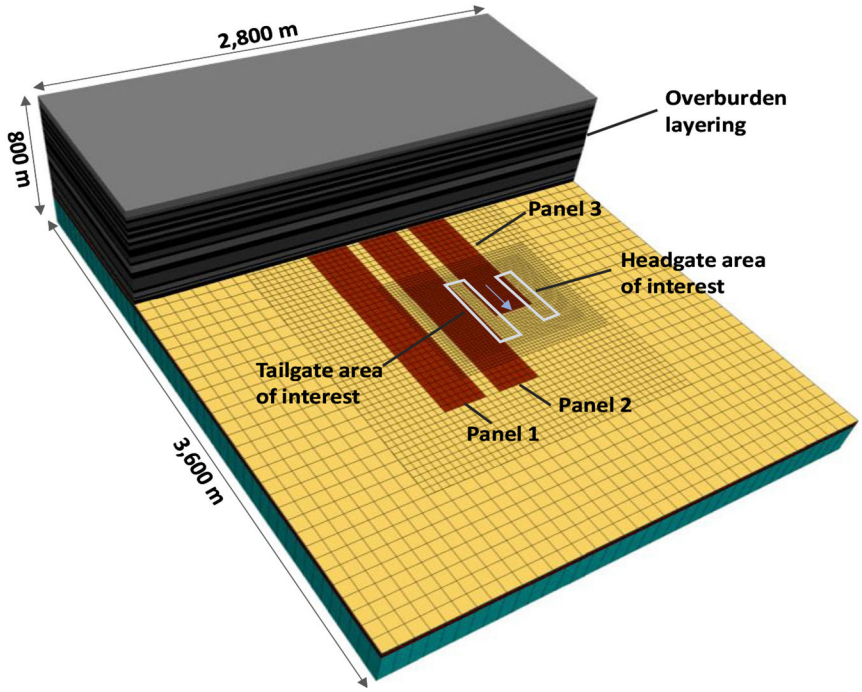

Fig. 7.

General layout of a district-scale model. Three longwall panels are shown with the first two panels fully extracted and the third panel being mined

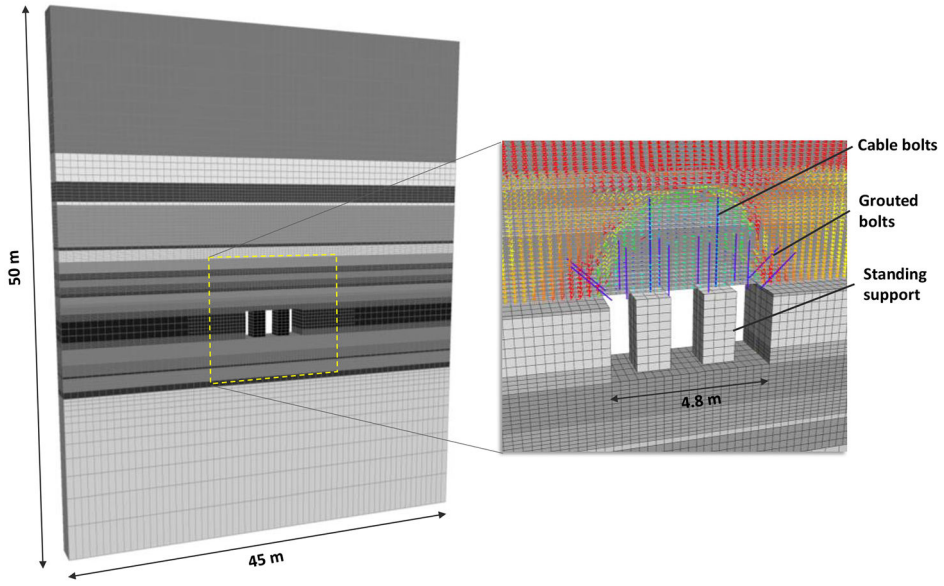

Fig. 8.

Layout of an entry-scale model showing dimensions, strata layering, and the entry location with standing supports. The inset shows a partial cutaway view of the entry, standing supports, bolts, and cable bolts. The principal stress distribution in the roof is also shown which illustrates the dome of reduced stress where the strata have yielded and fractured

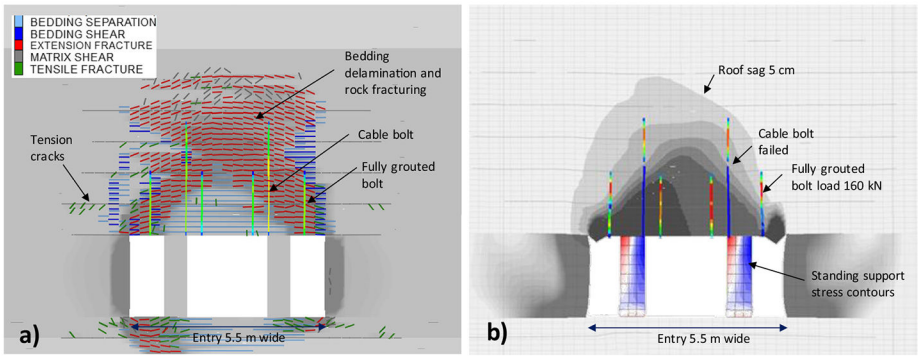

Fig. 9.

Example of FLAC3D numerical model results of entry and support response to longwall-induced loading: **a** showing rock failure modes, and **b** showing roof deformation and support response

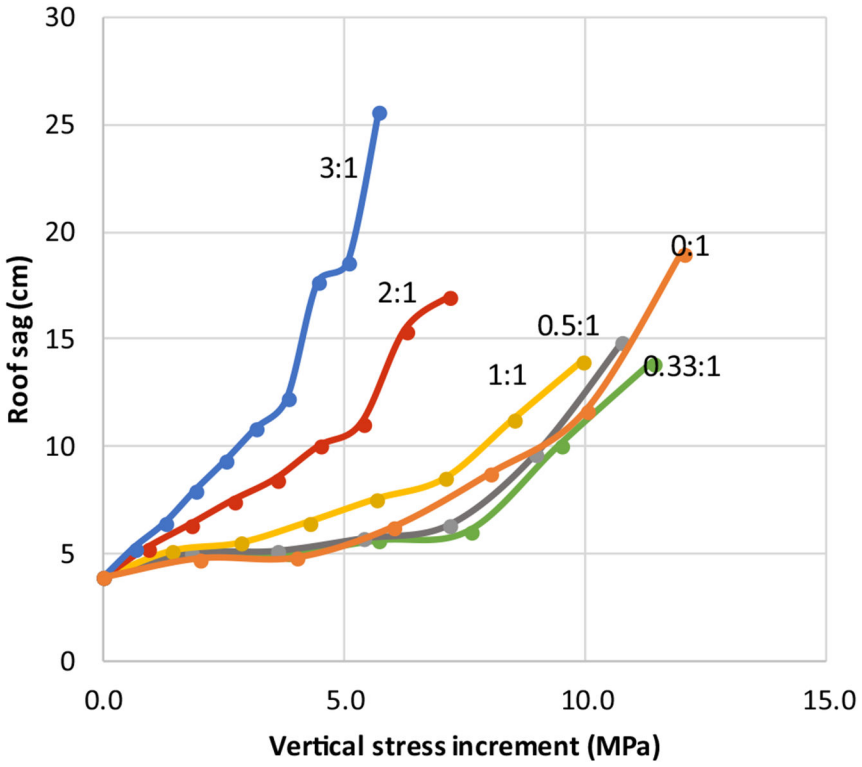

Fig. 10.

The impact of the ratio of longwall-induced, horizontal-to-vertical stress on roof sag predicted by numerical models of a gateroad in the Pittsburgh coal bed

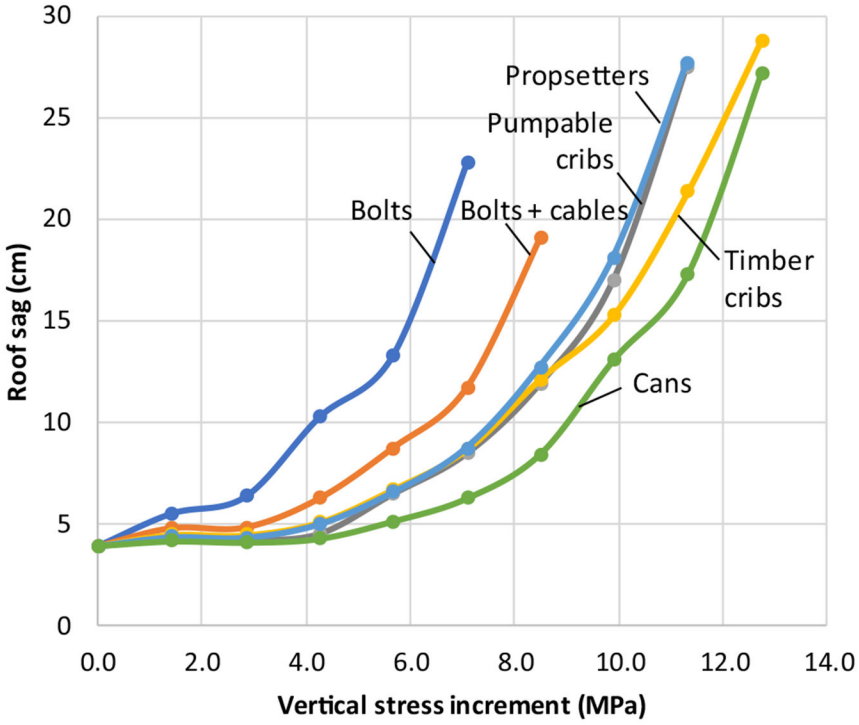

Fig. 11.

The effect of different types of roof support on roof sag predicted by numerical models of a gateroad in the Pittsburgh coal bed

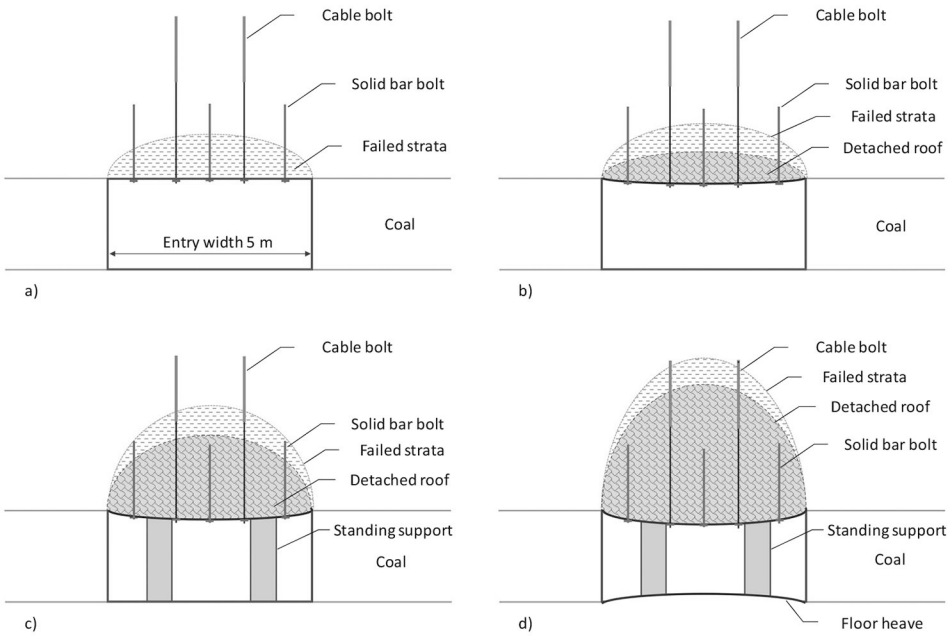

Fig. 12.

Conceptual sketches showing stages of failing roof and detached roof formed over a gateroad entry in response to increasing longwall-induced loads

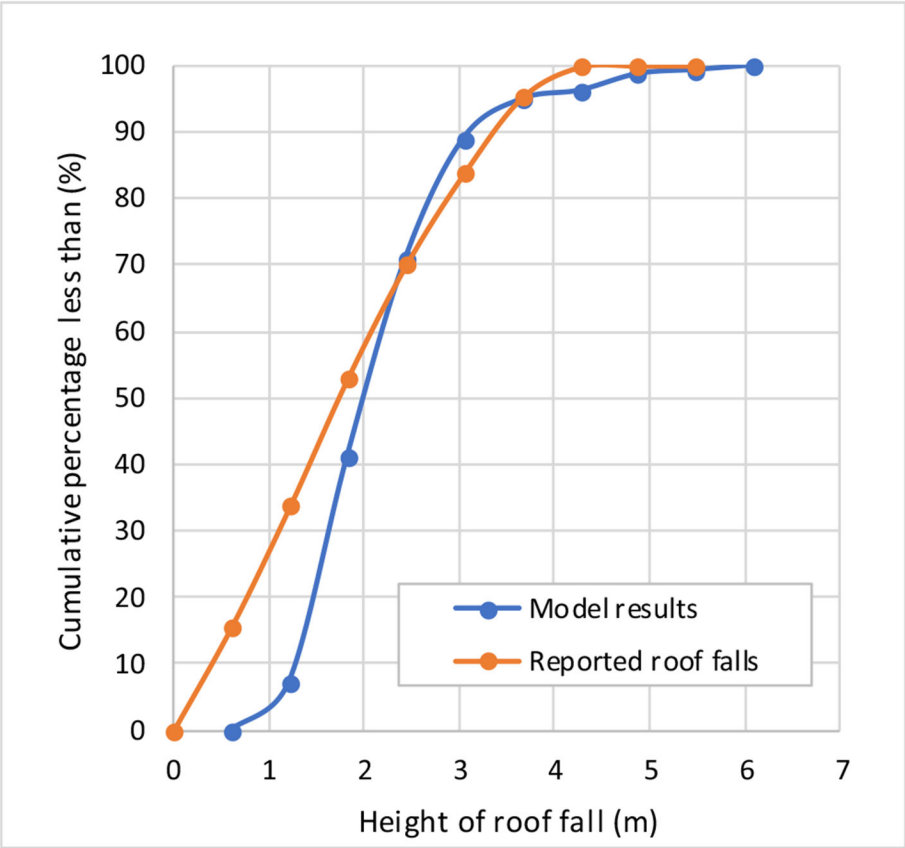

Fig. 13.
Comparison of reportable roof-fall heights in coal mines to numerical-model-predicted height of detached roof

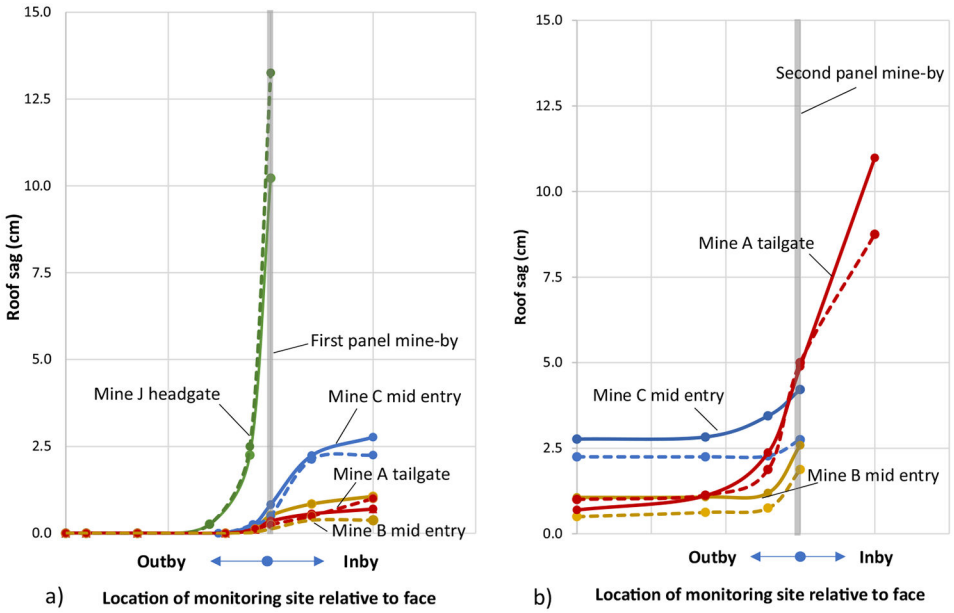

Fig. 14.

Comparison of measured roof sag (dashed lines) and calculated roof sag for: **a** first panel mine-by and **b** second panel mine-by using calculation procedures presented in this paper

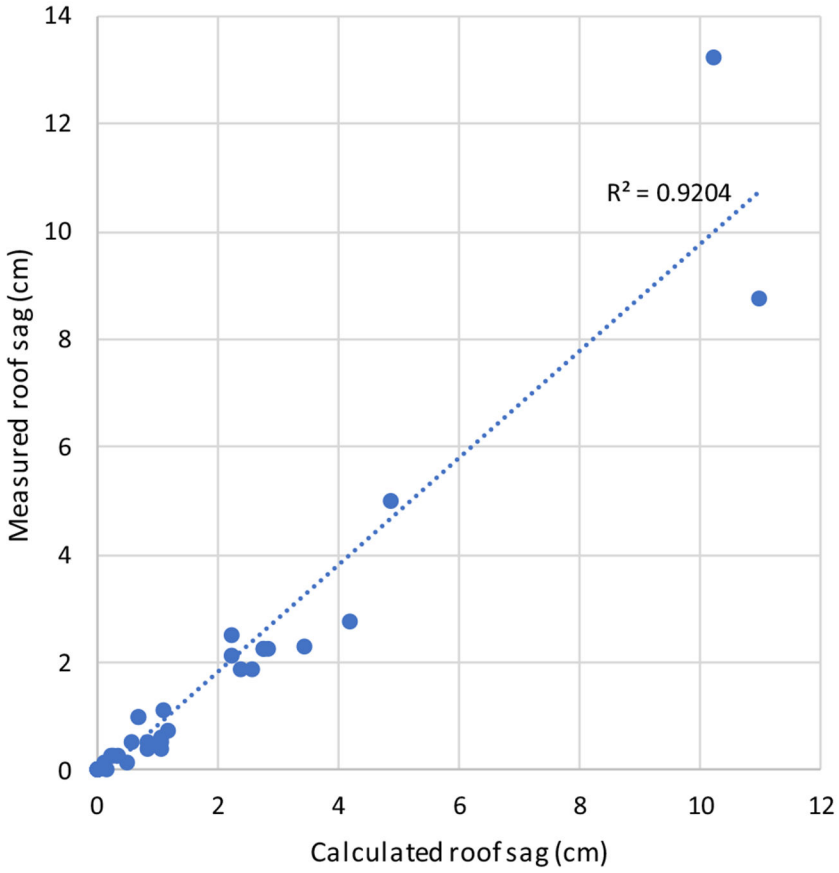

Fig. 15.

Correlation between calculated roof sag and measured roof sag at four gateroad monitoring sites

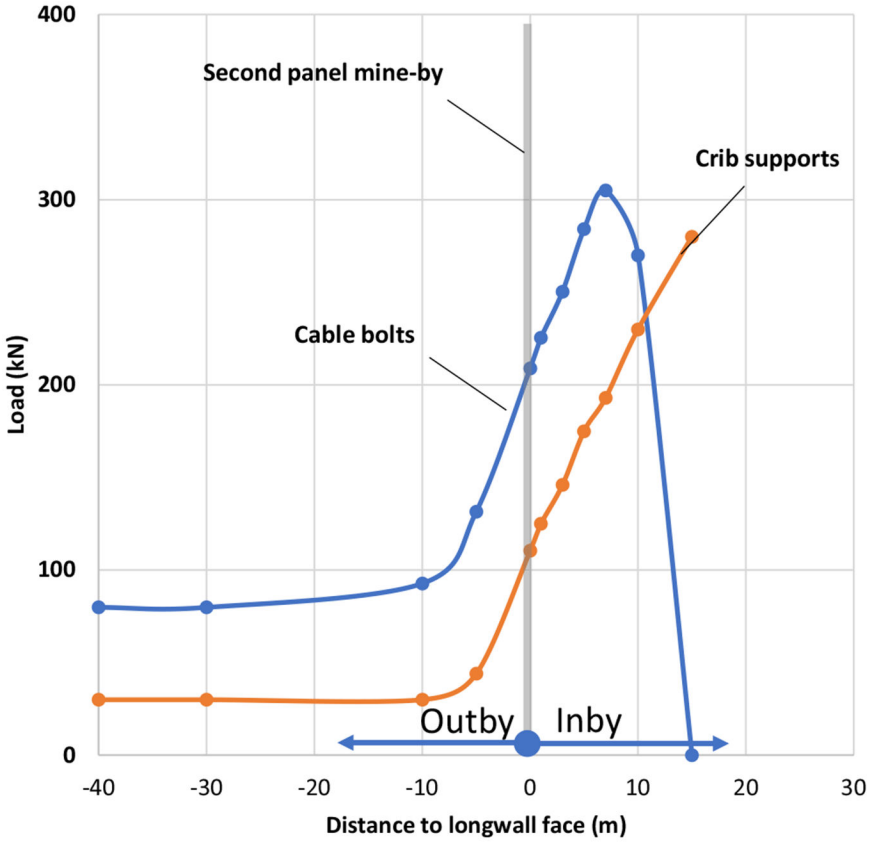

Fig. 16.

Bolt loads and standing support response calculated for the tailgate of mine A as the second panel mines by

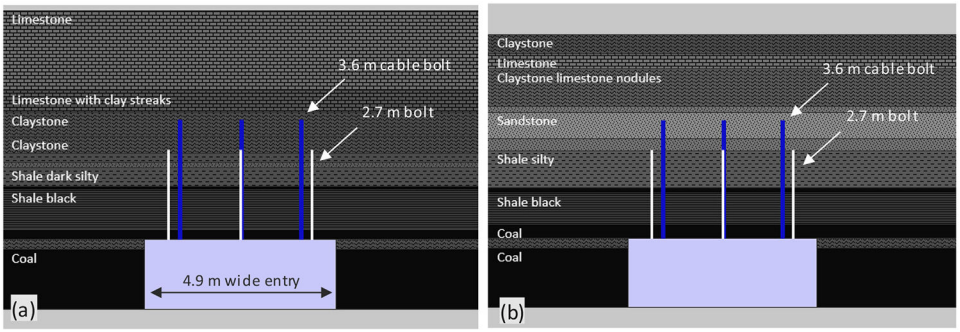

Fig. 17.

Schematic illustration of roof geology, entry location, and belt entry roof reinforcement, **a** transitional geology at location of headgate roof fall and **b** normal geology at location of NIOSH monitoring site. Darker shading indicates lower rock strength

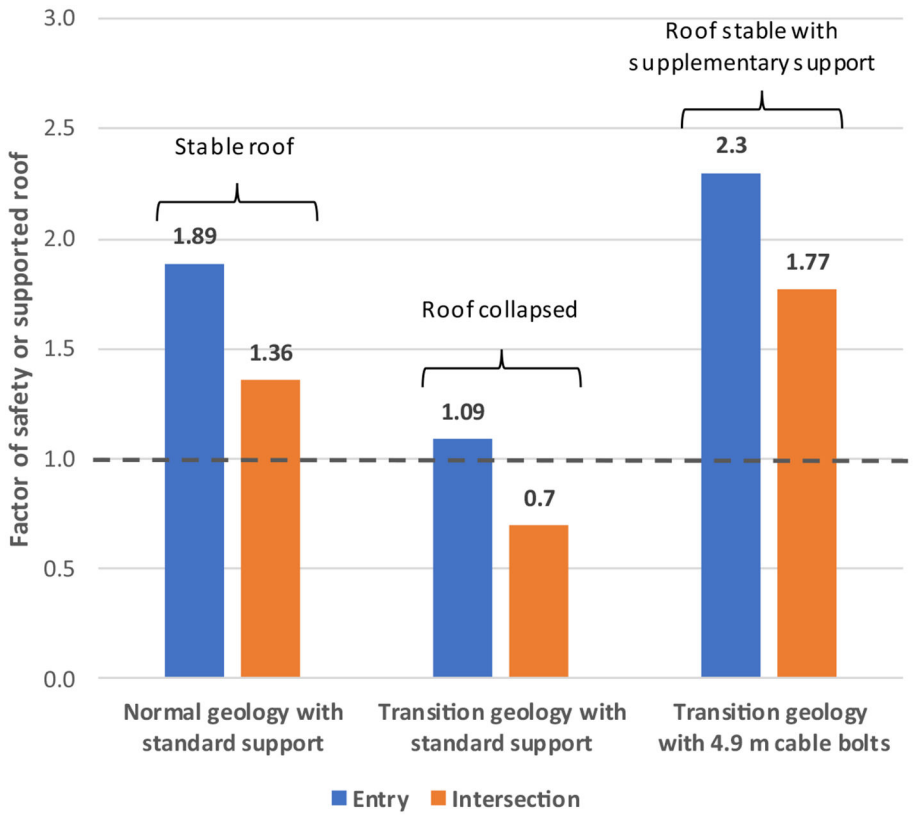

Fig. 18.

Stability of the longwall headgate belt entry and intersections under maximum loading, at the headgate corner

Table 1

Summary longwall dimensions and support systems used at six NIOSH gateroad monitoring sites

Mine label, location and coal bed mined	Depth of cover	Panel width and gateroad layout	Intrinsic roof support in monitored entry	Standing support in monitored entry
A: Northern WV, Lower Kittanning	180 m	366 m wide panel three entries: equal pillars 30 × 46 m centers	Tailgate: four 1.8 m fully grouted bolts in rows 1.2 m apart with two 1.8 m bolts at 45 deg at roof corners on every second row. Two 3 m passive cable bolts with 1.2 m resin grout on every row on steel straps.	Tailgate: two rows of 9-point wood cribs at 2.4 m centers
B: Southern VA, Pocahontas	670 m	214 m wide panel four entries: two yield pillars 15.2 × 40 m and central abutment pillar at 53 × 132 m centers	No. 2 entry: four 1.8 m tensioned and grouted roof bolts in rows 1.2 m apart with two 3.6 m cable bolts with 1.2 m resin grout between every second row of bolts.	No. 2 entry: two rows of 60 cm cans on 2.4 m centers
C: Western PA, Pittsburgh	260 m	488 m wide panel three entries: equal pillars Pillars: 30 × 56 m centers	No. 2 entry: alternating rows of three and two 1.8 m fully grouted bolts with center 4.9 m cable bolt every alternate row and steel channel on every row.	No. 2 entry: one row engineered wood cribs at 2.4 m centers
D: Central CO, D seam*	680 m	244 m wide panel three entries: equal pillars 28 × 61 m centers	Tailgate: four 1.8 m fully grouted blots in rows 1.2 m apart with 14-gauge steel straps and 8-gauge welded screen. Three 3.6 m cable bolts are installed in rows 2.4 m apart.	Tailgate: two rows of 76 cm pumpable cribs at 2.4 ft spacing
E: Western PA, Pittsburgh	180 m	312 m wide panel three entries: equal pillars 30 × 51 m centers	Crosscut: three 2.4 m long combination bolts with 1.2 m resin in rows 1.2 m apart and three 3.6 m cable bolts also with 1.2 m resin grout between rows primary bolts	None (site was in a crosscut)
F: Northern WV, Pittsburgh	305 m	357 m wide panel three entries: unequal pillars Pillars 35 × 42 m and 30 × 84 m centers	No. 2 Entry: three 2.7 m resin assisted combination bolts in rows 1.2 m apart installed on a steel strap with a central 3.6 m cable bolt every 2.4 m	Single row of 4-point timber cribs spaced 2.4 m apart

Table 2

Examples of material properties used to model intact rock and bedding within strata units

Type	Laboratory-scale UCS (MPa)	Elastic modulus (GPa)	Friction angle (deg.)	Field-scale cohesion (MPa)	Field-scale tensile strength (MPa)	Bedding friction angle (deg.)	Bedding cohesion (MPa)
Limestone 1	140	31.51	42	18.08	8.12	32	9.5
Limestone 2	100	26.86	42	12.91	5.80	28	6.7
Sandstone 1	80	17.60	37	11.57	4.64	30	6.0
Sandstone 2	60	14.74	35	9.06	3.48	25	3.4
Shale 1	40	11.88	25	7.39	2.32	10	2.4
Shale 2	30	10.45	20	6.09	1.74	7	1.7
Claystone 1	20	9.02	20	4.06	1.16	5	0.5
Claystone 2	10	7.59	20	2.03	0.58	5	0.1

Table 3

Properties for modeling fully grouted no. 6 solid bar bolts

Property	Value
Diameter	19 mm
Yield strain	9%
Steel modulus	200 GPa
Shear bond cohesion	500 kN/m
Normal bond cohesion	0.175 MPa
Shear bond stiffness	9.0×10^5 kN/m/m
Normal bond stiffness	8.0×10^5 kN/m/m
Shear bond softening rate (debonding)	240 kN/m/m

Table 4

Geologic scenarios evaluated in parametric studies

Description	Depth range (m)
Kittanning coal bed (mine A)	180 to 240 m
Pocahontas coal bed (mine B)	600 m
Pittsburgh coal bed (mine C)	240 m
Colorado D-seam (mine D)	360 m
Pittsburgh coal bed (mine E)	230 m
Weak immediate roof test	180 to 300 m
Weak main roof test	180 to 300 m
Uniform weak roof test	180 to 300 m
Moderate roof test	180 to 600 m
Strong roof test	180 to 600 m

Table 5

Average work capacity of some standing support types

Support type	Average work capacity (kN m/cm)
9-point timber crib	3.39
60 cm (24″) engineered timber crib	6.78
25 cm (10″) engineered timber prop	2.71
66 cm (30″) pumpable crib	5.50
60 cm (24″) can-type support	9.67

Table 6

Strength properties of roof strata used in the case study analysis

Rock type	UCS (MPa)	CMRR bedding rating
Coal	20.0	25
Claystone	18.0	20
Claystone with limestone nodules	24.0	30
Shale gray silty medium bedded	42.0	30
Shale gray thin bedded	42.0	20
Shale dark thin bedded with clay	31.0	20
Sandstone medium bedded	31.0	45
Sandstone thin bedded shale streaks	48.0	25
Limestone with clay streaks	45.0	35
Limestone	60.0	45